Water isotopologues as a quantitative paleosalinity proxy

Allegra N. LeGrande[1] and Gavin A. Schmidt[1]

Received 12 August 2010; revised 7 June 2011; accepted 29 June 2011; published 30 September 2011.

[1] Paleosalinity reconstructions are a goal of paleoceanographic study because of their potential to provide insight into past ocean circulation. While temperature reconstructions have been assessed by using multiple independent proxies, the skill of existing salinity reconstructions remains poorly quantified. We examine the applicability of two different approaches using a set of coupled water isotope–enabled general circulation model experiments as a numerical analog for the real climate system. These simulations for the Holocene, at roughly 1000 year time steps, explicitly track variability in both the water isotopologues and salinity. Our simulations suggest that quantitative reconstructions of past salinity variability based solely on inferred $\delta^{18}O_{sw}$ variability have very large errors and uncertainties. However, we find that paired $\delta^{18}O_{sw}$ and δD variability (from combining biomarker and calcite proxies) holds promise for providing better quantitative estimates of salinity variability.

Citation: LeGrande, A. N., and G. A. Schmidt (2011), Water isotopologues as a quantitative paleosalinity proxy, *Paleoceanography*, *26*, PA3225, doi:10.1029/2010PA002043.

1. Introduction

[2] The reconstruction of paleosalinity has long been a target of paleoclimate study since ocean salinity is a key factor in ocean density and circulation, and is also indicative of the regional hydrology. No direct measures of past salinity variability are currently available, and thus efforts have relied on indirect proxy indicators of past salinity. Water isotopologues in seawater (δD and $\delta^{18}O_{sw}$: δ in per mil units $\equiv (R_{sample}/R_{standard} - 1)*1000$) are intrinsically linked to salinity since surface freshwater exchanges are important in determining the variability of both. The two are regionally linearly related [*Fairbanks*, 1989], leading to the widespread use of $\delta^{18}O_{sw}$ as a proxy for past salinity [*Craig and Gordon*, 1965; *Duplessy et al.*, 1991].

[3] Seawater oxygen isotope concentration is preserved in carbonate from organisms such as foraminifera and corals, contributing to its use as a proxy for paleoceanographic conditions. Carbonate $\delta^{18}O$ concentration is controlled by both the temperature of seawater during formation (≈ -0.2‰ $\delta^{18}O_{sw}$ per °C), the isotopic composition of seawater, and species-dependent "vital effects." Given an independent temperature proxy (e.g., Mg/Ca in calcite), past variability in $\delta^{18}O_{sw}$ can be inferred from foraminifera and corals, allowing for estimations of past changes in salinity and ocean circulation [*Peña et al.*, 2008; *Rostek et al.*, 1993; *Schmidt et al.*, 2004; *Stott et al.*, 2004].

[4] The assumption that $\delta^{18}O_{sw}$ archives provide a quantitative measure of past salinity variability is problematic. As pointed out by *Craig and Gordon* [1965], water undergoes further fractionation and transportation after evaporation, giving an extra degree of freedom to water isotope variability over salinity variability. Temporal paleosalinity variability is typically inferred by a simple division of the past $\delta^{18}O_{sw}$ variability by the modern regional spatial $\delta^{18}O_{sw}$ to salinity relationship/covariability [*Rostek et al.*, 1993; *Stott et al.*, 2004]. This method assumes that the mechanisms (discussed below) that are the most important in determining the covariability of these two tracers within a region are the same mechanisms that control covariability through time.

[5] Previous work has suggested that during large changes in past climate, such as the last glacial maximum, 21,000 years ago, the $\delta^{18}O_{sw}$ to salinity relationship would have varied principally through the significant impact of land ice on the $\delta^{18}O_{sw}$ of runoff and alteration of the extent and amount of sea ice [*Rohling and Bigg*, 1998; *Schmidt*, 1999]. However, it is possible that other changes in climate and the hydrological balance could impact this relationship. Orbital variability, for instance, can cause large shifts in atmospheric circulation, as well [*Braconnot et al.*, 2007].

[6] Putting aside the complexities of reconstructing paleosalinity; $\delta^{18}O$ is fundamentally a tracer of the hydrologic cycle. The wide range of variability in freshwater $\delta^{18}O$ allows the determination of the relative proportion of water from multiple sources in both the ocean and atmosphere [e.g., *Khatiwala et al.*, 1999; *Masson-Delmotte et al.*, 2008; *Meredith et al.*, 1999; *Noone*, 2008]. In the ocean, $\delta^{18}O$ tracks regional freshwater balance and water mass exchange through surface ocean fluxes and ocean circulation [*Jacobs et al.*, 1985; *Skinner et al.*, 2003]. Fluxes of freshwater (e.g., precipitation, evaporation, and river input) affect the concentration of both $\delta^{18}O_{sw}$ and salinity yielding strong, but only regionally coherent correlations between the two in most of the ocean [*Craig and Gordon*, 1965; *Fairbanks*

[1]NASA Goddard Institute for Space Studies and Center for Climate Systems Research, Columbia University, New York, New York, USA.

0883-8305/11/2010PA002043

et al., 1992; *LeGrande and Schmidt*, 2006]. In the modern ocean, $\delta^{18}O_{sw}$ has been used as a tracer for sea ice melt, glacial and river runoff, deep ocean water masses, and deep water formation processes [*Strain and Tan*, 1993]. However, transport and additional fractionation in the atmosphere and other processes, such as sea ice formation, that affect seawater $\delta^{18}O$ and salinity differently make variations in $\delta^{18}O_{sw}$ more complicated than salinity variations, and limit good spatial correlations between $\delta^{18}O_{sw}$ and salinity to regional scales [*LeGrande and Schmidt*, 2006]. However, neither the equivalence of spatial and temporal correlations, nor the constancy of temporal correlations over long time scales during different mechanisms of climate change has been established, indeed, much evidence exists that these are not likely to be equivalent in general [*Rohling and Bigg*, 1998; *Schmidt et al.*, 2007; *Werner et al.*, 2000].

[7] In the atmosphere, the oxygen isotopic composition of precipitation $\delta^{18}O$ is a product of the initial composition of $\delta^{18}O$ in the water vapor of an air parcel and the amount of rain out and mixing of that air parcel along its path [*Dansgaard*, 1964]. It correlates well to surface air temperature at mid to high latitudes and may approximate the amount of precipitation at low latitudes over short time periods over or near oceans [*Rozanski et al.*, 1993]. Variability of precipitation $\delta^{18}O$ can influence $\delta^{18}O_{sw}$ in areas where there is significant glacial melt and river runoff [*Jacobs et al.*, 1985].

[8] The tropical hydrologic cycle is "closed" to first order (i.e., most of what evaporates in the tropics rains out in the tropics, making the average $\delta^{18}O$ of the two similar), and this results in shallow $\delta^{18}O_{sw}$ to salinity relationships [*Fairbanks et al.*, 1992; *LeGrande and Schmidt*, 2006]. (Details are in section 2.) The relatively small amount of "leakage" out of the tropics occurs at midtroposphere levels, and the isotopic composition of this "leaking" water sets the freshwater end-member for the extratropics. Input of freshwater from glacial melt and river runoff is also important to determining freshwater end-members locally. The tropical Atlantic and tropical Pacific are also strongly influenced by interocean exchange of freshwater (including over the Isthmus of Panama), and the isotopic composition of the vapor exchanged is important to determining freshwater end-members in each of these two regions as well [*Benway and Mix*, 2004]. Processes that control the distribution of rainfall on land, interocean exchange of water, and export of water vapor from the tropics could change on longer time scales, affecting the temporal relationship.

[9] Isotope-enabled general circulation models (GCMs) can act as numerical laboratories for assessing the strength and validity of assumptions made in paleoclimate reconstructions. The use of these models lies not in their imperfect realization of the climate system, but in their inclusion of many more factors than can be incorporated into reconstructions. Should assumptions about covariability not be supported in an appropriate model simulation, they are unlikely to be valid in the (more complex) real world. Interpretations of ice core isotope thermometry have benefited enormously from results drawn from atmospheric GCMs [*Charles et al.*, 1994; *Hoffmann et al.*, 2005; *Jouzel et al.*, 1994; *Werner et al.*, 2000]. Coupled ocean-atmosphere models have not been used as widely, but they enable more complex assumptions related to paleoceanographic proxies to be examined [*LeGrande and Schmidt*, 2006; *Schmidt et al.*, 2007].

[10] In this paper, we examine the mechanisms that control the variability of water isotopologues and salinity in a coupled GCM and provide a quantitative assessment of the skill of two different techniques for estimating paleosalinity from water isotope variability. The first technique, described above, uses modern $\delta^{18}O_{sw}$ to salinity spatial relationships to infer paleosalinity. The second technique was suggested by *Rohling* [2007] and pairs both past $\delta^{18}O_{sw}$ and δD_{sw} (deuterium, ^2H) variability to estimate paleosalinity. We evaluate ocean water isotopologue and salinity variability on decadal and millennial time scales using results from eight Holocene time slice, equilibrium simulations, roughly 1000 years apart, from the fully coupled, isotope-enabled GCM, Goddard Institute for Space Studies (GISS) ModelE-R. The skill and details of the model in simulating the Holocene are presented by *LeGrande and Schmidt* [2009].

[11] The primary driver of climate change over the Holocene is thought to be related to changes in the orbital configuration. Perihelion shifts during the Holocene changes Northern Hemisphere seasonality, with the maximum difference from today occurring in the early Holocene. Remnant ice sheets and long-term consequences of the deglaciation also influence early Holocene climate. In the tropics, rainfall was likely shifted northward in the early Holocene, with some indications that its intensity was greater, with diminishing intensity and southward migration through to the modern. The western tropical Pacific is thought to have been more saline in the early Holocene [*Stott et al.*, 2004], and El Niño–Southern Oscillation variability is thought to have had smaller magnitude than today [*Brown et al.*, 2008; *Chiang et al.*, 2009]. The tropical Atlantic was thought to be more saline as well [*Schmidt et al.*, 2004]. Terrestrial proxies indicate warmer Northern Hemisphere summers, and reduced sea ice extent [*Davis et al.*, 2003; *Kaufman et al.*, 2004; *Masson et al.*, 2000], although ocean temperature trends appear to vary as a function of latitude, warming through the Holocene in the tropics, while cooling in more polar latitudes [*Lorenz et al.*, 2006]. Overall, the Holocene is thought to be a relatively stable period of time spanning the last 10,000 years, making it a telling period to assess the skill of the two paleosalinity reconstruction methods.

2. Methods

[12] GISS ModelE-R is a fully coupled atmosphere/ocean GCM. The experiments here use the M20 version of ModelE whose horizontal resolution is 4° × 5°, with a 20 vertical layer atmosphere up to 0.1 hPa height coupled to the 13-layer Russell Ocean model at the same horizontal resolution [*Hansen et al.*, 2007; *Schmidt et al.*, 2007]. Atmospheric advection uses the quadratic upstream scheme, with 9 moments advected in addition to mean quantities, significantly enhancing the effective tracer resolution (to ~1.3° × ~1.6°). The ocean model is non-Boussinesq, mass conserving, and has a full free surface. Freshwater is treated in a "natural" way; that is, the addition of freshwater increases the free surface and reduces salinity purely through dilution. No equivalent salt fluxes or flux adjustments are used, allowing for the prognostic calculation of water isotope to salinity

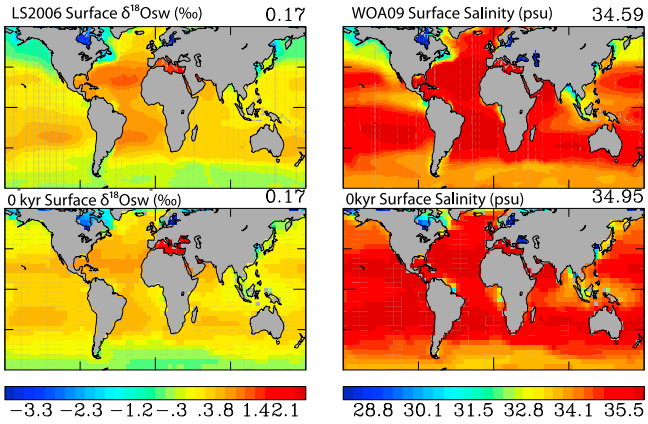

Figure 1. (top) Sea surface $\delta^{18}O_{sw}$ from *LeGrande and Schmidt* [2006] and salinity from *Antonov et al.* [2010]. (bottom) Simulated sea surface $\delta^{18}O_{sw}$ from the 0 kya (preindustrial) simulation of Goddard Institute for Space Studies ModelE-R and simulated surface salinity.

relationships. All boundary conditions and atmospheric composition in the control case are appropriate to the preindustrial period (circa 1880).

[13] Water tracers ($^1H_2^{16}O$, "normal" water; $^2H^1H\,^{16}O$, δD; $^1H_2^{18}O$, $\delta^{18}O$) are included in the atmosphere, land surface, sea ice, and ocean and are tracked through all stages of the hydrologic cycle. These isotopes are advected like water through the model, but at each phase change, an appropriate fractionation is performed.

[14] Eight "time slice" experiments were performed, giving roughly 1000 year temporal coverage across the Holocene: 0, 1, 2, 3, 4, 5, 6, and 9 kiloyears ago (kya). In each, greenhouse gas concentrations were adjusted based on ice core reconstructions, and seasonal insolation was changed as a function of changing orbital parameters. For the 9 kya experiment, a remnant Laurentide ice sheet was included, and mean ocean water salinity and $\delta^{18}O$ adjusted to account for ice volume (+0.33‰ equivalent to ~35 m of sea level) changes. Each experiment was run 500 years, reaching quasi equilibrium, and the last 100 years of the experiments are presented here.

3. Paleosalinity Reconstructions

[15] GISS ModelE-R does a reasonable job of simulating $\delta^{18}O_{sw}$ and salinity (Figure 1), with problems appearing as zonal smoothing of tracer gradients and too enriched (high) values in areas where the local freshwater balance is negative.

3.1. Holocene $\delta^{18}O_{sw}$ to Salinity Relationships

[16] The simulated regional spatial 0 kya $\delta^{18}O_{sw}$ to salinity slopes (Figure 2 and Table 1) follow those observed; the $\delta^{18}O_{sw}$ to salinity slope is greatest at midlatitudes and high northern latitudes, and shallower in the tropics and Southern Ocean [*LeGrande and Schmidt*, 2006]. Simulated $\delta^{18}O_{sw}$ matches observed $\delta^{18}O_{sw}$ reasonably well, except that simulated zonal gradients are too shallow, similar to other tracer fields [*Schmidt et al.*, 2007].

[17] Vigorous water recycling in the tropics yields a freshwater end-member there that is more enriched than in high latitudes and a very shallow $\delta^{18}O_{sw}$ to salinity gradient, typically 0.1 to 0.3‰/practical salinity unit (psu) [*LeGrande and Schmidt*, 2006]. The isotopic ratio in the small amount of water that leaves the tropics at a midtroposphere level is quite depleted, with $\delta^{18}O$ of −15 to −20‰ [*LeGrande and Schmidt*, 2009, Figure 8a]; it becomes the freshwater end-member for the extratropics [*Craig and Gordon*, 1965]. In the extratropics this end-member combined with depleted end-members from river input as well as a significant amount of water imported and exported from each region, yields steeper $\delta^{18}O_{sw}$ to salinity slopes, typically >0.5‰/psu [*Craig and Gordon*, 1965; *Fairbanks et al.*, 1992; *LeGrande and Schmidt*, 2006]. Since sea ice (weakly) preferentially incorporates $\delta^{18}O$ and excludes salt, yielding a (slightly) negative $\delta^{18}O_{sw}$ to salinity relationship, opposite of that observed in most other processes, we will exclude discussion of high-latitude $\delta^{18}O_{sw}$ to salinity relationships in this paper.

[18] Simulated modern relationships resemble those observed (Figure 2 and Table 1). For instance, the simulated tropical Atlantic relationship is shallow (~0.23–0.27‰/psu), but somewhat steeper than observed (0.15‰/psu). Simulated subtropical slopes are appropriately steeper than the tropical slopes at 0.4–0.6‰/psu, but sometimes shallower than observed. These simulated regional characteristics have remained largely unchanged, within decadal time scales or within a single time slice, across our Holocene experiments (Figure 3). The greatest exception occurs in the early Holocene, when highly depleted glacial runoff from the shrinking Laurentide Ice Sheet [*Carlson et al.*, 2008] combined with altered simulated Atlantic Ocean circulation, steepens $\delta^{18}O_{sw}$ to salinity relationships there.

[19] The above discussion focuses on the regional spatial relationship between $\delta^{18}O_{sw}$ and salinity. We now turn to the temporal relationships, simulated in this study. We illustrate these in detail at three discreet locations relevant to existing paleosalinity reconstructions: (1) the North Atlantic, (2) the western tropical Pacific, and (3) the eastern tropical Pacific (Figure 4). At the decadal scale, the local temporal relationship is usually similar to the regional spatial slope (varying as shown in Figure 3). However, this is not generally true for the longer time scales involved in paleosalinity reconstructions.

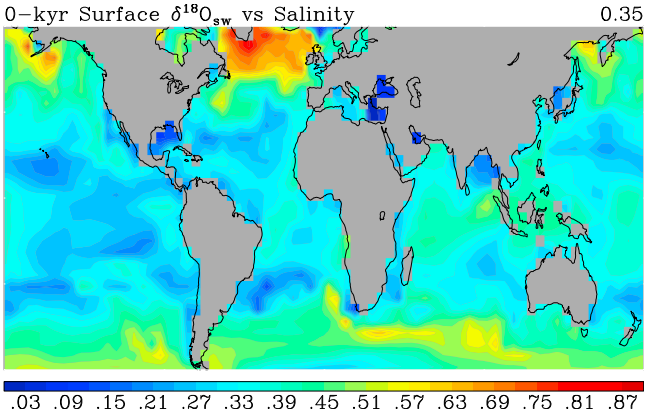

Figure 2. Local linear regression on decadal covariability between surface $\delta^{18}O_{sw}$ and salinity at 0 kya (preindustrial conditions) over a 100 year time period.

Table 1. Observed Slope (m) and Intercept (b) for Various Regions Compared to Simulated Slope (m) and Intercept (b) for the 0, 3, 6, and 9 kya Time Slices[a]

Region	Observed[b]		Model	0 (kya)				3 (kya)				6 (kya)				9 (kya)			
	m	b	Count	m	b	Qfit	σ_m	m	b	Qfit	σ_m	m	b	Qfit	σ_m	m	b	Qfit	σ_m
Arctic	0.48	−16.82	311	0.40	−14.49	0	0.01	0.40	−14.74	0	0.01	0.42	−15.33	0	0.01	0.51	−18.05	0	0.01
GIN Seas	0.33	−11.82	15	0.44	−15.86	0.62	0.11	0.41	−14.80	0.48	0.12	0.33	−12.30	0.46	0.12	0.62	−21.73	0.97	0.02
Baltic Sea	0.28	−8.73	3	0.43	−14.86	0.94	0.01	0.43	−14.87	0.94	0.01	0.43	−14.99	0.93	0.01	0.43	−14.80	0.93	0.01
Hudson Bay	0.42	−16.05	13	0.33	−12.41	0.85	0.04	0.34	−12.87	0.81	0.04	0.35	−13.21	0.82	0.04	NA	NA	NA	NA
Barents Sea	0.6	−20.71	36	0.60	−20.61	0	0.06	0.59	−20.44	0	0.06	0.58	−19.98	0.01	0.05	0.63	−21.66	0	0.06
North Atlantic	0.55	−18.98	122	0.48	−16.47	1	0.01	0.47	−16.35	1	0.01	0.47	−16.39	1	0.01	0.56	−19.32	1	0.01
Tropical Atlantic	0.15	−4.61	131	0.23	−7.61	1	0.01	0.24	−7.92	1	0.01	0.25	−8.47	1	0.01	0.27	−8.67	1	0.01
South Atlantic	0.51	−17.4	109	0.44	−15.20	1	0.00	0.44	−15.24	1	0.00	0.44	−15.38	1	0.00	0.44	−15.05	1	0.00
Mediterranean	0.28	−9.24	32	0.47	−16.12	0.89	0.02	0.46	−16.06	0.87	0.02	0.45	−15.38	0.87	0.02	0.41	−14.01	0.93	0.01
Southern Ocean	0.24	−8.45	385	0.50	−17.34	1	0.01	0.50	−17.45	1	0.01	0.47	−16.39	1	0.01	0.47	−16.10	1	0.01
North Pacific	0.44	−15.13	189	0.36	−12.36	1	0.01	0.38	−13.07	1	0.01	0.39	−13.44	1	0.01	0.43	−14.41	1	0.01
Tropical Pacific	0.27	−8.88	312	0.25	−8.58	1	0.00	0.24	−8.17	1	0.00	0.23	−7.82	1	0.01	0.23	−7.51	1	0.01
South Pacific	0.45	−15.29	209	0.35	−12.01	1	0.01	0.35	−12.05	1	0.01	0.35	−12.25	1	0.00	0.36	−12.22	1	0.00
Red Sea/Persian Gulf	0.31	10.81	3	0.21	−6.68	0.89	0.00	0.22	−6.94	0.9	0.00	0.21	−6.91	0.9	0.00	0.22	−6.80	0.91	0.00
North Indian	0.16	−5.31	154	0.27	−9.01	1	0.01	0.26	−8.86	1	0.01	0.26	−8.97	1	0.01	0.27	−8.87	1	0.00
South Indian			139	0.46	−15.78	1	0.01	0.45	−15.71	1	0.01	0.45	−15.56	1	0.01	0.45	−15.06	1	0.01

[a]For the simulated fields the quality of fit (Qfit) and sigma slope (σ_m) are provided. Count refers to the number of grid boxes used to determine the statistics in each time slice.
[b]As calculated by *LeGrande and Schmidt* [2006].

[20] At millennial time scales, using the 8 time slice simulations representing the course of the Holocene, the local temporal slope is frequently different than the regional spatial slope. In the North Atlantic location, the regression through mean millennial $\delta^{18}O_{sw}$ and salinity is the same at decadal time scales and during the Holocene as a whole (Figure 4a). This slope also fits with the $\delta^{18}O_{sw}$ and salinity values of the early Holocene which are influenced by the significant increase of $\delta^{18}O$ depleted freshwater drainage from the remnant Laurentide Ice Sheet. However, for the western tropical Pacific (Figure 4b), changes to $\delta^{18}O_{sw}$ are larger than those in salinity (relative to what would have been expected from the modern spatial relationship), resulting in a Holocene temporal slope that is over twice the modern annual to decadal temporal slope. This implies that paleosalinity reconstructions of the western tropical Pacific would infer too great of change in salinity given $\delta^{18}O_{sw}$ variability. The eastern tropical Pacific has the opposite behavior, as no changes occur in $\delta^{18}O_{sw}$, but small changes occur in salinity; the modulation here is linked to changes in water vapor transport from the Atlantic into the Pacific and to an increase (by ~8% in the early Holocene) of western flow into the western tropical Pacific.

[21] The simulations also suggest that the temporal slope is not constant. That is, the relative differences between salinity and $\delta^{18}O_{sw}$ given any two time slices (i.e., the slope between two time slices 0–3, 3–6, and 6–9 kya) are not the same in addition to varying significantly in sign and magnitude from the modern (local decadal/regional spatial) slope. This variability indicates that fine-scale quantitative salinity reconstructions may be exceptionally difficult given the variety of climate change drivers that have operated in the past.

[22] We illustrate the difference between the 0 kya decadal temporal slope and the Holocene temporal slope by repeating the single grid box analyses in Figure 4 globally for Figure 5 (shows the regression of the $\delta^{18}O_{sw}$ to salinity slope over the course of the Holocene (8 time slices)). To facilitate our understanding of the impact these differences

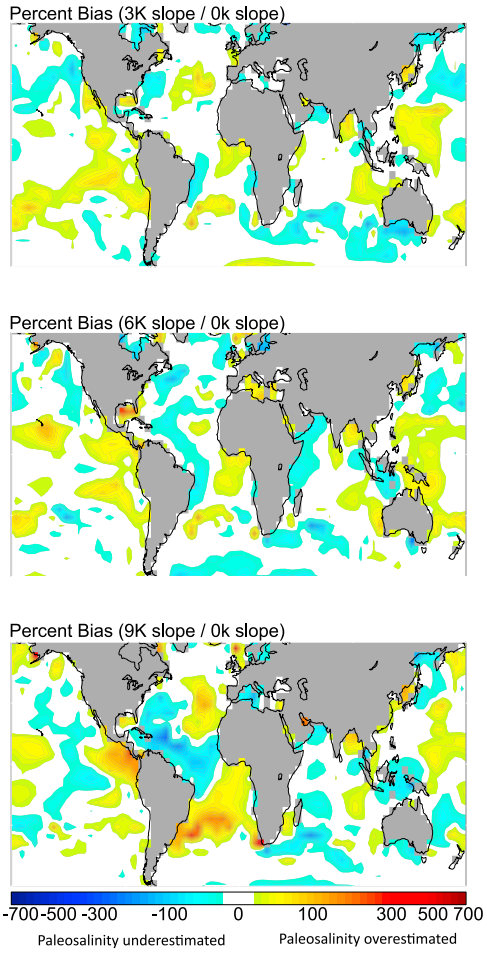

Figure 3. Percent bias of the local linear regression between surface $\delta^{18}O_{sw}$ and salinity at (top) 3, (middle) 6, and (bottom) 9 kya divided by the local linear regression at 0 kya (Figure 5). Places where the slope is unchanged compared to modern are uncolored.

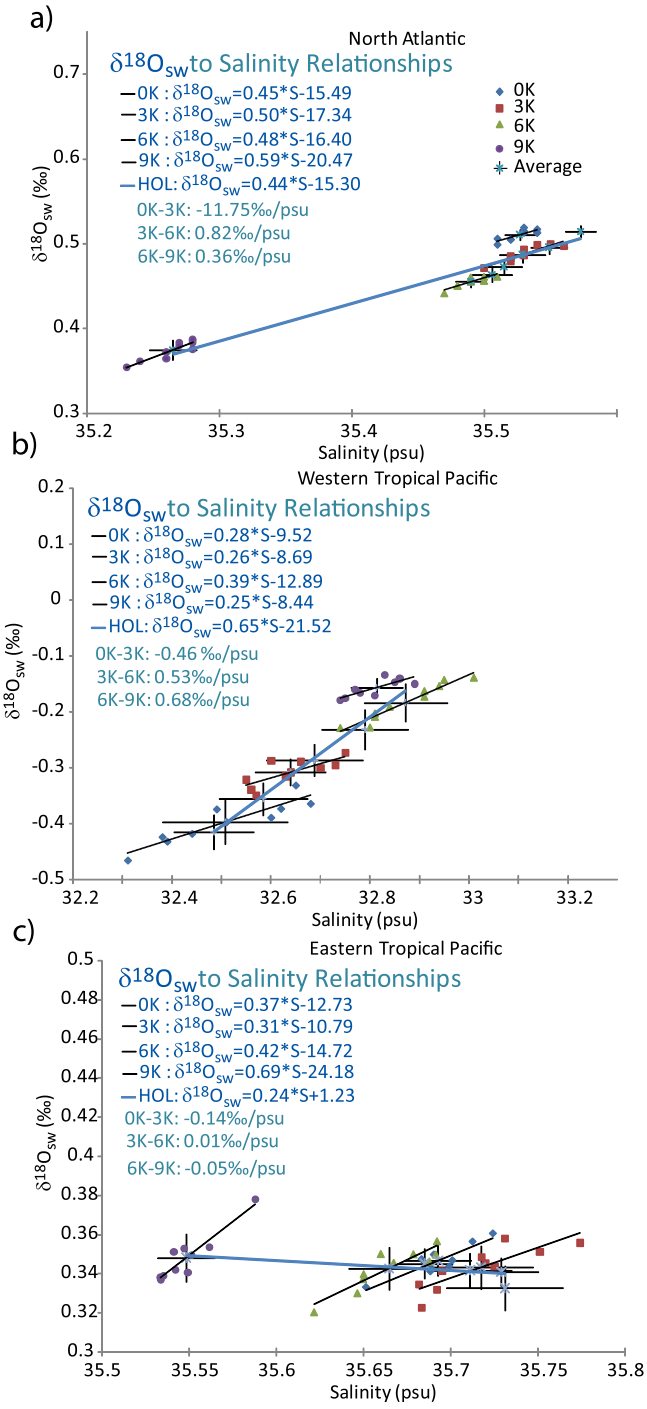

Figure 4. For three points in the ocean, the (a) North Atlantic, (b) western tropical Pacific, and (c) eastern tropical Pacific decadal linear regressions between surface $\delta^{18}O_{sw}$ and salinity at 0, 3, 6, and 9 kya with the regression through the mean value of all eight simulations printed over in blue. Note that this Holocene (HOL) slope is not equivalent to individual slopes between each time slice. Individual decadal averages appear for the 0 (blue diamonds), 3 (red squares), 6 (green triangles), and 9 kya (purple circles) cases; average values for all eight simulations appear in blue asterisks, with the 1σ variation about the mean printed on top.

have on millennial salinity reconstructions, we normalize Figure 5 by the modern decadal slope and present the data as percent bias. Here, for instance, a 100% bias means that the reconstructed salinity change using the $\delta^{18}O_{sw}$ to salinity slope is twice the simulated salinity change. Figure 5 shows the percent of error in using the local decadal slope instead of the (appropriate) millennial-scale slope to infer salinity from $\delta^{18}O_{sw}$. The reporting of quantitative reconstructions for the Holocene could be improved by including estimated errors determined from these simulations as shown in Figure 5. (For example, a western tropical Pacific reconstruction might contain additional error bars of 100–200%.) Even reporting qualitative reconstructed temporal changes in salinity can be misleading since the magnitude of change from one part of the record to the next may be very different.

[23] Figure 6 provides a quantitative sense of how this shift would impact paleosalinity reconstructions. (Note that Figure 6 is not intended to be used as error bars on paleosalinity reconstructions. Figure 5 is better suited for this purpose.) Figure 6 (top) shows "virtual" paleosalinity change at 9 kya; the 9 kya change in $\delta^{18}O_{sw}$ (adjusted for ice volume changes) is divided by the 0 kya $\delta^{18}O_{sw}$ to salinity relationship. This is the typical method used for paleosalinity reconstructions [*Peña et al.*, 2008; *Schmidt et al.*, 2004; *Stott et al.*, 2004]. Figure 6 (bottom) is the difference between this "virtual" salinity change and the simulated paleosalinity change at 9 kya. Again the western tropical Pacific stands out as a location where paleosalinity changes are overestimated (positively), and the tropical Atlantic to Gulf of Mexico have similarly large errors where paleosalinity changes are overestimated (negatively).

[24] Extra oceanic transport pathways are important even during the Holocene, in determining the temporal salinity to $\delta^{18}O_{sw}$ relationship. The impact of using a modern regional spatial salinity to $\delta^{18}O_{sw}$ slope to estimate the temporal slope is to yield paleosalinity change estimates that are too great in the tropical Atlantic and western tropical Pacific and too small in the eastern tropical Pacific (though here, the variability of $\delta^{18}O_{sw}$ is too small for the result to be significant). In the Caribbean, salinity changes are generally small and negative (compared to 0 kya). In contrast, $\delta^{18}O_{sw}$ here decreases more than would be anticipated given the modern 0.23–0.27‰/psu (0 kya, temporal relationship). In some locations, the western tropical Atlantic spatial slope is too shallow by a factor of 3 (Figure 5). In the western tropical Pacific, both salinity and $\delta^{18}O_{sw}$ are greater (compared to 0 k), and the $\delta^{18}O_{sw}$ gets heavier more quickly than salinity increases (predicted given the modern regional spatial 0.23–0.27‰/psu relationship, Figure 4c).

[25] These alterations in the tropical hydrologic cycle (and $\delta^{18}O_{sw}$ to salinity relationship) have repercussions for the extratropics as well. For instance, when poleward transport of heavy water decreases, the freshwater end-members for the extratropics becomes lighter (and vice versa, Figure 4). As such, the slopes within individual time slices either spatial or temporal at the decadal scale, can remain relatively unchanged while the intercept (or freshwater end-member) changes. The millennial temporal slope changes ultimately reflect the relative changes in the mean salinity and $\delta^{18}O_{sw}$ values of a region.

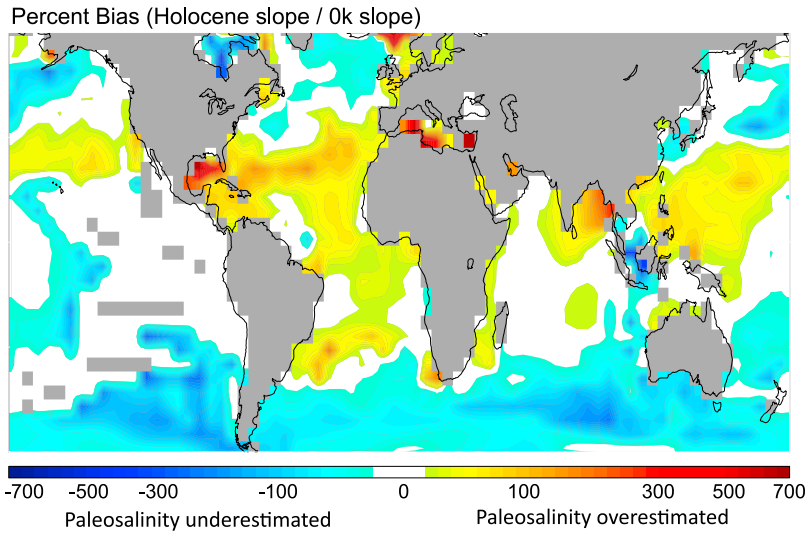

Figure 5. Variations in Holocene (0–9 kya) slope of surface $\delta^{18}O_{sw}$ versus salinity normalized by 0 kya slopes. For each grid box, a linear regression is performed through the 100 year average surface $\delta^{18}O_{sw}$ and salinity (eight points); this regression is normalized by the surface $\delta^{18}O_{sw}$ versus salinity slope (Figure 1). The percent bias of this ratio is plotted above: warm colors indicate places where paleosalinity would be overestimated using the 0 kya slope, and cool colors indicate places where paleosalinity would be underestimated using the 0 kya slope.

3.2. Quantifying Uncertainties in Finding Salinity

[26] Previous work has attempted to quantify the structural and analytical source of errors in standard paleosalinity estimates [*Rohling and Bigg*, 1998; *Schmidt*, 1999].The most significant sources of error were found to be the uncertainty in the linear regressions used and the potential uncertainty in the spatial slopes. For the mid-Holocene where no ice volume related corrections are needed, the uncertainty in paleosalinity measurements can be estimated as from *Schmidt* [1999, equation (8)] where the errors in salinity reconstruction (σ_S) can be approximated using the inverse of the $\delta^{18}O_{sw}$ to salinity relationship (G), the goodness of fit of the mixing line (σ_{ml}), the errors in $\delta^{18}O_{sw}$ (σ_w), the errors in the freshwater end-member (σ_F) and of Δ_{wi}, related to the offset between $\delta^{18}O_{sw}$ (δ_w), and (when in the tropics) less the offset between tropical and ocean mean waters (δ_{offset}) all scaled by the $\delta^{18}O$ of the paleofreshwater end-member in the (δ'_F):

$$\sigma_S^2 \approx \frac{1}{G^2}\left(\sigma_{ml}^2 + \sigma_w^2 + \Delta_{wi}^2\sigma_F^2\right)$$

$$\Delta_{wi} = \frac{\delta_w - \delta_{offset}}{\delta'_F}$$

[27] The equation can usefully be applied separately in the tropics and the midlatitudes with slightly different values of G and σ_{ml} in both cases (tropics: G = 0.3‰/psu, σ_{ml} = 0.13; midlatitudes: G = 0.5‰/psu, σ_{ml} = 0.2). σ_w depends on the methodology with which the $\delta^{18}O_{sw}$ was derived, while Δ_{wi} and σ_F are related to the structural uncertainty in the appropriate slope. In the absence of this uncertainty, this equation estimates that paleosalinities anomalies are at best only going to be (1 σ) 0.6–1.1 psu (midlatitudes) and 0.9–1.8 psu (tropics) depending on the source of the temperature used in calculating $\delta^{18}O_{sw}$.

[28] However, given the magnitude of systematic change in the slope in time seen in our simulations, the uncertainties in derived Holocene salinities increases beyond these structural/analytical errors by up to 300% in some regions (Figure 5). (To be clear, a 2 psu reconstruction of paleosalinity anomaly to modern from the modern $\delta^{18}O_{sw}$ to salinity relationship given the simulated calculating $\delta^{18}O_{sw}$ actually

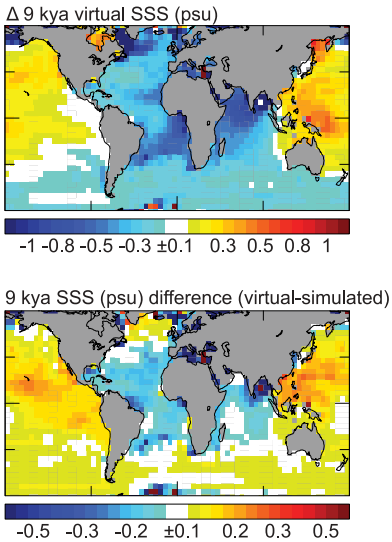

Figure 6. (top) "Virtual" sea surface salinity constructed by dividing the (9–0 kya) surface $\delta^{18}O_{sw}$ by the modern surface $\delta^{18}O_{sw}$ to salinity relationship at 0 kya (preindustrial conditions), the typical method used for paleosalinity reconstructions. (bottom) The difference between simulated sea surface salinity change at 9 kya and the "virtual" sea surface salinity change.

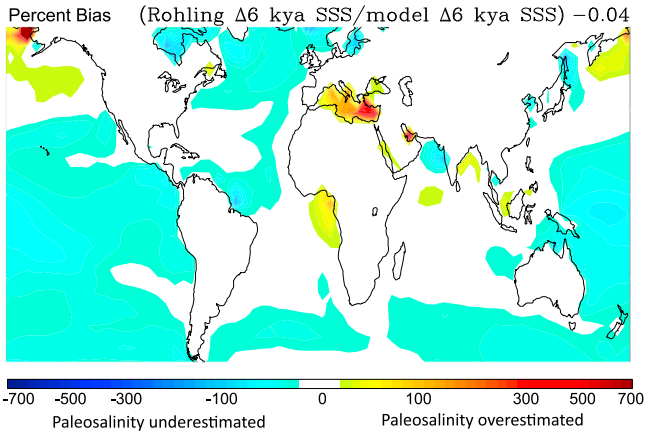

Figure 7. Percent bias of the technique by *Rohling* [2007] for estimating paleosalinity (through use of both oxygen and deuterium isotopes) and the corresponding salinity change.

corresponds to only a 1 psu simulated salinity change in addition to the ~0.6–1.8 psu structural/analytical error.) If the results here are robust though, it may be possible to use the model-derived temporal slopes directly in the calculation (with their own error bar) to reduce the eventual uncertainty.

3.3. Constraining Paleosalinity With Additional Tracers

[29] Clearly, the simulations demonstrate that applying the modern spatial slope to infer past salinity changes regionally can yield very high biases, upward of 100–200% in the Western tropical Pacific, western tropical Atlantic, and Caribbean. However, these estimates only use information contained within the in oxygen isotopes in carbonate. Recently, it has been suggested that pairing information from both these proxies and hydrogen isotope variability from biomarkers could yield better estimates for paleosalinity (if the isotopic composition of surface water vapor fluxes is little changed from a reference period) [*Rohling*, 2007].

[30] Following *Rohling* [2007], we apply the following relationship for determining paleosalinity to the simulated preindustrial surface salinity (S0), preindustrial surface δD (δD_{0sw}), preindustrial surface $\delta^{18}O$ ($\delta^{18}O_{0sw}$), change in surface seawater δD ($\Delta\delta D_{sw}$), change in surface seawater $\delta^{18}O$ ($\Delta\delta^{18}O_{sw}$), and assuming a preindustrial meteoric water line slope of 8 (λ_0) with a deuterium excess of 10 (d_0):

$$S = S_0\left(1 + \frac{\Delta\delta D_{sw} - \lambda_0\Delta\delta^{18}O_{sw}}{\delta D_{0sw} - \lambda_0\delta^{18}O_{0sw} - d_0}\right)$$

[31] Assuming that we have perfect information about the δD changes, as previously, we can calculate the estimated salinity change and compare it to the simulated salinity change during the mid-Holocene (Figure 7). We find that this technique generally has much smaller biases, with most estimates off by only 20–30%. However, some areas, such as the Mediterranean Sea still have sizable biases. This offset is likely due to changes in the freshwater end-member entering the region, which factors into the denominator of the above equation. For instance, in the eastern Mediterranean, speleothem records (pairing $\delta^{18}O_{calcite}$ and δD of fluid inclusions) indicate that the deuterium excess of water vapor (and perhaps the isotopic composition of water vapor) changed during the mid-Holocene to modern (M. Bar-Matthews, personal communication, 2008). This observation is also consistent with our simulated circulation changes that indicate a greater influx of Atlantic water vapor (thus fluxes were less purely drawn from Mediterranean sources).

[32] The patterns of offset in using only the oxygen isotopes (Figure 5) and both oxygen and deuterium isotopes (Figure 7) are quite different. The oxygen isotope-only based changes tend to be overestimated in the western tropical Pacific, western tropical Atlantic, and underestimated in the eastern tropical Pacific. The pairing of the two water isotopologues largely produces smaller biases (relatively to the oxygen isotopes alone) that are more global in extent. Pairing the two water isotopologues together thus appears to be a promising way of extracting paleosalinity from past climate records, although it would require that another proxy (for δD) be acquired at each core site from alkenones or other biomarkers [e.g., *Pahnke et al.*, 2007] and which would need to be calibrated to the water isotope composition at the time of calcification of the $\delta^{18}O$.

4. Regional Ocean Water Mass Changes

[33] In order to understand why changes occur in both salinity and water isotopologues within each region, we diagnose the full budget of water imported and exported in each region. We focus here on two regions for which there are published paleosalinity reconstructions for the Holocene. Regional definitions follow *LeGrande and Schmidt* [2006], except that the tropical Pacific is partitioned into eastern and western regions, with the division occurring at 175°W and the Indian Ocean is subdivided across the equator.

[34] First, we consider the western tropical Pacific where salinity and $\delta^{18}O_{sw}$ are higher compared to 0 kya, and paleosalinity estimates based on modern spatial covariability of the two here would tend to be too high. In the early Holocene (EH) (9 kya), precipitation over the western tropical Pacific is reduced by 3%, while evaporation increases by 0.5% (with progressively smaller changes relative to 0 kya into the mid Holocene (MH) (6 kya) and late Holocene (LH) (3 kya)). This region has ~5% increased transport from the eastern tropical Pacific in the MH to EH, but less than a 1% change at 3 kya, while eastward exchange was reduced (ΔLH: −6%, ΔMH: −2%, ΔEH: −9%). Flow into this region from the northern Pacific (recirculation) is progressively enhanced from the early to late Holocene, with an increased transport of 73% at 9 kya, with only an 8% increase in return back northward compared to 0 kya. The flux into the western tropical Pacific from the North Pacific in the mid-Holocene is of similar magnitude to the precipitation flux, while in the preindustrial it is only roughly half of the precipitation flux. Exchange of water from below the thermocline is also progressively enhanced from the late to early Holocene, with the mid-Holocene having 8% greater upwelling and 15% greater downwelling. Westward flow through the Indonesian Seaways is progressively reduced from the late to early Holocene, with advection diminished by 12% at 9 kya. Transport of waters southward into the South Pacific is progressively increased from the late (8%) to early Holocene (15%).

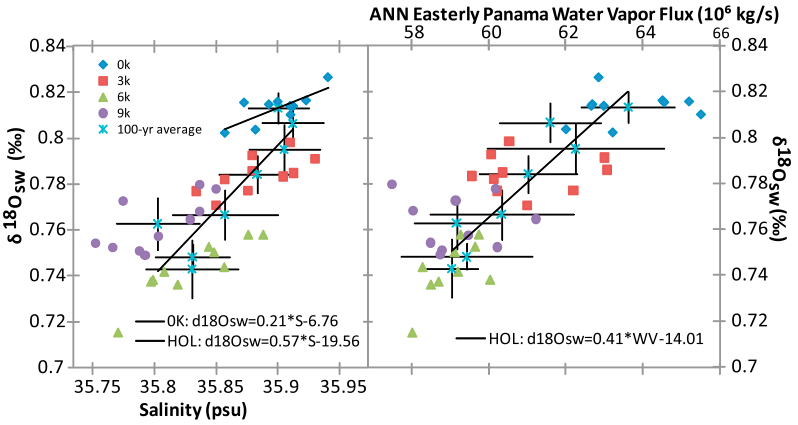

Figure 8. (left) Decadal mean $\delta^{18}O_{sw}$ and salinity for Gulf of Mexico for 0 (blue), 3 (red), 6 (green), and 9 kya (purple). The 100 year average $\delta^{18}O_{sw}$ and salinity (cyan stars) are plotted with the 1 σ error overlaid for 0, 1, 2, 3, 4, 5, 6, and 9 kya. Regressions are for (1) 0 kya preindustrial decadal points and (2) 100 year average of all eight Holocene simulations. For Figure 8 (left), the value is 0.57/0.21–1 = 1.7 (paleosalinity change is prone to overestimation). (right) Decadal mean $\delta^{18}O_{sw}$ and annually averaged easterly water vapor flux into Panama ($\delta^{18}O$ of water vapor ~−8‰) for 0 (blue), 3 (red), 6 (green), and 9 kya (purple). The 100 year average $\delta^{18}O_{sw}$ and annually averaged easterly water vapor flux over Panama (cyan stars) are plotted with the 1 σ variation overlaid for 0, 1, 2, 3, 4, 5, 6, and 9 kya. The regression is through 100 year average points, showing positive correlation between the two.

[35] In short, more water enters the western tropical Pacific from the North and East, while more exits westward; surface freshwater input is reduced; and deep exchange increases. These collectively work both to make this area more saline and enriched in $\delta^{18}O$ (compared to 0 kya), as well as to pull the salinity $\delta^{18}O_{sw}$ curve off its preindustrial spatial relationship. To focus, we compare the MH to 0 kya, the EH and LH scale. The average salinity difference between the western tropical Pacific and northern Pacific is 0.3 psu, while the average $\delta^{18}O_{sw}$ is 0.15‰ less in the North Pacific, while the eastern tropical Pacific is only 0.15 psu more saline, but 0.2‰ more enriched. In the preindustrial, the salinity $\delta^{18}O_{sw}$ slope is 0.37‰/psu; a 0.15–0.2‰ $\delta^{18}O_{sw}$ change would thus imply a 0.4–0.55 psu salinity change. Increases in evaporation ($\delta^{18}O$ 0 kya: −4.3‰, $\delta^{18}O$ MH: −4.5‰) and decreases in precipitation ($\delta^{18}O$ 0 kya: −5.4‰, $\delta^{18}O$ MH: −5.2‰) both work to salinify and enrich western tropical Pacific waters. At both time slices, the P-E $\delta^{18}O$ difference is small (0 kya: 1.1‰; MH: 0.7‰), which serves to maintain a shallow salinity $\delta^{18}O_{sw}$ slope within each time slice. These precipitation and evaporation $\delta^{18}O$ values represent freshwater end-members for the region. They are similar, though not identical, pushing the salinity $\delta^{18}O_{sw}$ curve at millennial time scales toward steeper slopes at decadal and shorter time scales. Alterations in ocean advection driven by shifting wind bands following changes in sea surface temperature patterns and the thermal equator play the most important role in setting the mean salinity and isotopic composition of seawater.

[36] Turning to the Caribbean, a few percent less water is exported across the Isthmus of Panama to the Pacific at the MH than at 0 kya (Figure 8). Changing cross-isthmus transport affects both the Atlantic and Pacific basins, but the smaller volume of water in the Atlantic, and particularly in Gulf of Mexico intensifies the impact alterations in cross-isthmus transport there. In the model, the freshwater end-member for the Gulf of Mexico (basin wide average) is around −5‰. This freshwater end-member is less depleted than that observed, −8.4‰ [*Benway and Mix*, 2004; *LeGrande and Schmidt*, 2006]. The isotopic composition of water vapor exported to the Pacific is ≈−12 to −13‰ across all the Holocene experiments. Modulating the transport of this more highly depleted water vapor exported from the Atlantic (than the local salinity to $\delta^{18}O_{sw}$ end-member) has the effect of steepening tropical Atlantic salinity to $\delta^{18}O_{sw}$ relationships (150–300% within the Gulf of Mexico) and dampening (very slightly) eastern tropical Pacific salinity to $\delta^{18}O_{sw}$ slopes (Figure 5). This result suggests that $\delta^{18}O_{sw}$ analyses in the Gulf of Mexico and Caribbean may not be suitable for determining quantitative salinity changes (using this method, at least), but may be useful for assessing changes in interbasin exchange of water. This exchange can have important repercussions for setting the average salinity of the Atlantic basin and thus in determining the strength of meridional overturning circulation at higher latitudes.

5. Discussion

[37] Reconstructing paleosalinity changes has long been a goal of paleoceanographic studies but in the absence of direct measures for salinity, a variety of indirect proxy techniques have been proposed. Significant biases in paleosalinity estimates are introduced using the technique of applying modern regional, spatial slopes to infer the local, temporal covariability of $\delta^{18}O_{sw}$ and salinity. In places such as the tropical Atlantic and western tropical Pacific, paleosalinity change estimates over the Holocene may be overestimated by 100–300%. This bias means that the changes in salinity are much more modest than implied by the changes in $\delta^{18}O_{sw}$ variability. These biases are in addition to any noise or artifacts introduced into the estimated $\delta^{18}O_{sw}$ variability during the subtraction of the temperature signal from the $\delta^{18}O_{calcite}$

signal as well as structural/analytical errors in the determination of the spatial slopes.

[38] The departure of the local, temporal slope from the regional, spatial slope over the course of the Holocene is driven primarily by orbital changes. Other drivers of climate change over glacial-to-interglacial time scales may produce a different pattern of temporal slopes. On longer time scales, there is also the addition of orographic, ice sheet–related, greenhouse gas, and geographic changes. It is not clear whether these would exaggerate these orbitally driven biases or not. Future work will include periods with these changes to assess the impact of changes in other boundary conditions.

[39] Fundamentally, atmospheric pathways for exchange of water are the cause of variability of $\delta^{18}O_{sw}$ to salinity relationships. They are also the reason that spatial and temporal covariability are not equivalent. At short annual to decadal time scales, regional evaporation and precipitation and input from major rivers combined with ocean dynamics are important at setting the covariability. This can be generalized to mean that the location of the region (i.e., tropical, subtropical, and greater river input) is the most important factor in the regional spatial $\delta^{18}O_{sw}$ to salinity relationship. For instance, most water evaporated from the tropics remains in the tropics making the $\delta^{18}O$ of evaporate and precipitate are quite similar and relatively heavy and yielding shallow tropical $\delta^{18}O_{sw}$ to salinity relationships. At higher latitudes, freshwater is imported in the atmosphere and exported from ocean regions; depleted water from river systems is also introduced. These yield steeper extratropical $\delta^{18}O_{sw}$ to salinity relationships.

[40] On millennial time scales, changes in the interbasin exchange of water become the driver of $\delta^{18}O_{sw}$ to salinity covariability. The flux of water across the Isthmus of Panama is important in setting the average $\delta^{18}O_{sw}$ and salinity of the Atlantic and Pacific Oceans. Variability in this exchange in our experiments is crucial in determining the Holocene $\delta^{18}O_{sw}$ to salinity relationships. Orbital-scale variability in the patterns of rainfall, e.g., which river catchment basin receives rain from which ocean basin and into which ocean basin it returns, is also important in determining the freshwater end-member of the $\delta^{18}O_{sw}$ to salinity relationship.

[41] In areas like the North Atlantic, the input of glacial meltwater is important in making the local $\delta^{18}O_{sw}$ to salinity slope steep: the 9 kya case has ~40% greater input of depleted runoff (−13 to −14‰ including both glacial and river sources) compared to the 0 kya. The change in the amount of this important freshwater end-member from the early to late Holocene drives the Holocene temporal slope. Similarly, in the modern, the input of depleted runoff is an important control on the $\delta^{18}O_{sw}$ to salinity slope at decadal time scales within each time slice. To maintain a similar slope at millennial time scales, (1) either no (or exactly identical) changes can occur in the processes that set the mean values of $\delta^{18}O_{sw}$ and salinity or (2) a "coincidental" process must occur on millennial time scales that yields a similar relationship between the two. The latter occurs over the course of the Holocene in the North Atlantic. Here, at the *century* time scale, variability in glacial runoff is not significant enough to cause a different covariability in the $\delta^{18}O_{sw}$ to salinity relationship in the 0 kya through 6 kya time slices; Figure 4a shows that over this time period, there are only very small changes in salinity with some variability in $\delta^{18}O_{sw}$. At 9 kya, there are significant changes to glacial runoff, and thus the millennial-scale slope in $\delta^{18}O_{sw}$ to salinity is similar when that earliest time period is considered. Given this sensitivity, paleosalinity reconstructions in regions subject to large variations in glacial meltwater are likely to be problematic.

[42] *Rohling* [2007] suggested that pairing reconstructions of seawater $\delta^{18}O$ with seawater δD might improve paleosalinity estimates. This technique in general has much smaller biases (<40%) and patterns of bias that are completely different to the paired temperature proxy $\delta^{18}O_{calcite}$ technique, at least using our simulations. This method holds promise for providing a better assessment of past salinity variability. However, this technique requires that material be obtained from fundamentally different proxy archives, and this pairing could introduce additional errors. Variability of $\delta^{18}O$ is obtained through measuring zooplankton (foraminifera) calcite shells $\delta^{18}O$, while δD must be obtained from alkenones or other biomarkers. Alkenones are captured from calcareous algae (coccoliths). But, there could be ecological biases introduced by combining these two records; that is, the seasonal bloom of the two species need not be the same. Furthermore, the relatively small size of coccoliths compared to foraminifera means that they are much more susceptible to transportation away from the "formation" site to the site where they are deposited. Other confounding factors include differences in dissolution and bioturbation at the core site.

[43] Despite the complications of solely using $\delta^{18}O_{sw}$ for quantitative paleosalinity reconstructions, it remains a good qualitative tool for estimating relative changes in past salinity. Furthermore, constraining other signals captured in $\delta^{18}O_{sw}$, such as interbasin exchange of water (e.g., over the Isthmus of Panama), make this past climate proxy useful for estimating changes in other parts of the hydrologic cycle.

6. Conclusion

[44] Variability in $\delta^{18}O_{sw}$ tracks changes in the hydrologic cycle. However, interpretations of this proxy as being solely controlled by ocean salinity or changes in precipitation are likely to be too simplistic.

[45] Here, we have shown that the simulated regional spatial $\delta^{18}O_{sw}$ to salinity slopes, which are usually similar to decadal and interannual slopes, are not equal to the simulated millennial slopes over the Holocene because the variability in $\delta^{18}O_{sw}$ and salinity has different causes at these time scales. On longer time scales, mean alterations in atmospheric pathways for water (changes to the hydrologic cycle) alter $\delta^{18}O_{sw}$, causing its relationship to salinity to change. For paleosalinity reconstructions, modern regional relationships are not appropriate scaling factors for interpreting $\delta^{18}O_{sw}$ as salinity. Combining variability in both water isotopologues, $\delta^{18}O_{sw}$ and δD, may allow for a better estimation of paleosalinity variability.

[46] **Acknowledgments.** We would like to thank NASA Modeling, Analysis, and Prediction Program for assistance with climate modeling and NASA GISS for institutional support. A.N.L. was supported by NSF ATM 07-53868 and NOAA NA10OAR4310126.

References

Antonov, J. I., D. Seidov, T. P. Boyer, R. A. Locarnini, A. V. Mishonov, H. E. Garcia, O. K. Baranova, M. M. Zweng, and D. R. Johnson (2010), *World Ocean Atlas 2009*, vol. 2, *Salinity*, *NOAA Atlas NESDIS*, vol. 69, 184 pp., NOAA, Silver Spring, Md.

Benway, H. M., and A. C. Mix (2004), Oxygen isotopes, upper-ocean salinity, and precipitation sources in the eastern tropical Pacific, *Earth Planet. Sci. Lett.*, *224*(3–4), 493–507, doi:10.1016/j.epsl.2004.05.014.

Braconnot, P., et al. (2007), Results of PMIP2 coupled simulations of the Mid-Holocene and Last Glacial Maximum—Part 2: Feedbacks with emphasis on the location of the ITCZ and mid- and high latitudes heat budget, *Clim. Past*, *3*(2), 279–296, doi:10.5194/cp-3-279-2007

Brown, J., A. W. Tudhope, M. Collins, and H. V. McGregor (2008), Mid-Holocene ENSO: Issues in quantitative model-proxy data comparisons, *Paleoceanography*, *23*, PA3202, doi:10.1029/2007PA001512.

Carlson, A. E., A. N. LeGrande, D. W. Oppo, R. E. Came, G. A. Schmidt, F. S. Anslow, J. M. Licciardi, and E. A. Obbink (2008), Rapid early Holocene deglaciation of the Laurentide ice sheet, *Nat. Geosci.*, *1*(9), 620–624, doi:10.1038/ngeo285.

Charles, C. D., D. Rind, J. Jouzel, R. D. Koster, and R. G. Fairbanks (1994), Glacial-Interglacial changes in moisture sources for Greenland: Influences on the ice core record of climate, *Science*, *263*(5146), 508–511, doi:10.1126/science.263.5146.508.

Chiang, J. C. H., Y. Fang, and P. Chang (2009), Pacific climate change and ENSO activity in the mid-Holocene, *J. Clim.*, *22*(4), 923–939, doi:10.1175/2008JCLI2644.1.

Craig, H., and L. I. Gordon (1965), Deuterium and oxygen 18 variations in the ocean and the marine atmosphere, in *Stable Isotopes in Oceanographic Studies and Paleotemperatures*, edited by E. Tongiorgi, pp. 9–130, Cons. Naz. delle Ric., Spoleto, Italy.

Dansgaard, W. (1964), Stable isotopes in precipitation, *Tellus*, *16*, 436–468, doi:10.1111/j.2153-3490.1964.tb00181.x.

Davis, B. A. S., S. Brewer, A. C. Stevenson, and J. Guiot (2003), The temperature of Europe during the Holocene reconstructed from pollen data, *Quat. Sci. Rev.*, *22*(15–17), 1701–1716, doi:10.1016/S0277-3791(03)00173-2.

Duplessy, J. C., L. Labeyrie, A. Juilletleclerc, F. Maitre, J. Duprat, and M. Sarnthein (1991), Surface salinity reconstruction of the North Atlantic Ocean during the last glacial maximum, *Oceanol. Acta*, *14*(4), 311–324.

Fairbanks, R. G. (1989), A 17,000-year glacio-eustatic sea level record: Influence of glacial melting rates on the Younger Dryas event and deep-ocean circulation, *Nature*, *342*, 637–642, doi:10.1038/342637a0.

Fairbanks, R. G., C. D. Charles, and J. D. Wright (1992), Origin of global meltwater pulses, in *Radiocarbon After Four Decades: An Interdisciplinary Perspective*, edited by R. E. Taylor, A. Long, and R. S. Kra, pp. 473–500, Springer, New York.

Hansen, J., et al. (2007), Climate simulations for 1880–2003 with GISS modelE, *Clim. Dyn.*, *29*(7–8), 661–696, doi:10.1007/s00382-007-0255-8.

Hoffmann, G., M. Cuntz, J. Jouzel, and M. Werner (2005), How much climatic information do water isotopes contain? A systematic comparison between the AIEA/GNIP isotope network and the ECHAM 4 atmospheric general circulation model, in *Isotopes in the Water Cycle: Past, Present, and Future of a Developing Science*, edited by P. K. Aggarwal, J. R. Gat, and K. F. O. Froehlich, pp. 303–320, Springer, Dordrecht, Netherlands.

Jacobs, S. S., R. G. Fairbanks, and Y. Horibe (1985), Origin and evolution of water masses near the Antarctic continental margin: Evidence from $H_{218}O/H_{216}O$ ratios in seawater, in *Oceanology of the Antarctic Continental Shelf*, *Antart. Res. Ser.*, vol. 43, edited by S. S. Jacobs, pp. 59–85, AGU, Washington, D. C.

Jouzel, J., R. D. Koster, R. J. Suozzo, and G. L. Russell (1994), Stable water isotope behavior during the last glacial maximum: A general circulation model analysis, *J. Geophys. Res.*, *99*(D12), 25,791–25,801, doi:10.1029/94JD01819

Kaufman, D. S., et al. (2004), Holocene thermal maximum in the western Arctic (0–180°W), *Quat. Sci. Rev.*, *23*(5–6), 529–560, doi:10.1016/j.quascirev.2003.09.007.

Khatiwala, S. P., R. G. Fairbanks, and R. W. Houghton (1999), Freshwater sources to the coastal ocean off northeastern North America: Evidence from $H_2^{18}O/H_2^{16}O$, *J. Geophys. Res.*, *104*(C8), 18,241–18,255, doi:10.1029/1999JC900155

LeGrande, A. N., and G. A. Schmidt (2006), Global gridded dataset of the oxygen isotopic composition in seawater, *Geophys. Res. Lett.*, *33*, L12604, doi:10.1029/2006GL026011.

LeGrande, A. N., and G. A. Schmidt (2009), Sources of Holocene variability of oxygen isotopes in paleoclimate archives, *Clim. Past*, *5*(3), 441–455, doi:10.5194/cp-5-441-2009.

Lorenz, S. J., J. H. Kim, N. Rimbu, R. R. Schneider, and G. Lohmann (2006), Orbitally driven insolation forcing on Holocene climate trends: Evidence from alkenone data and climate modeling, *Paleoceanography*, *21*, PA1002, doi:10.1029/2005PA001152.

Masson, V., et al. (2000), Holocene climate variability in Antarctica based on 11 ice-core isotopic records, *Quat. Res.*, *54*(3), 348–358, doi:10.1006/qres.2000.2172.

Masson-Delmotte, V., et al. (2008), A review of Antarctic surface snow isotopic composition: Observations, atmospheric circulation, and isotopic modeling, *J. Clim.*, *21*(13), 3359–3387, doi:10.1175/2007JCLI2139.1.

Meredith, M. P., K. E. Grose, E. L. McDonagh, K. J. Heywood, R. D. Frew, and P. F. Dennis (1999), Distribution of oxygen isotopes in the water masses of Drake Passage and the South Atlantic, *J. Geophys. Res.*, *104*(C9), 20,949–20,962, doi:10.1029/98JC02544.

Noone, D. (2008), The influence of midlatitude and tropical overturning circulation on the isotopic composition of atmospheric water vapor and Antarctic precipitation, *J. Geophys. Res.*, *113*, D04102, doi:10.1029/2007JD008892.

Pahnke, K., J. P. Sachs, L. Keigwin, A. Timmermann, and S. P. Xie (2007), Eastern tropical Pacific hydrologic changes during the past 27,000 years from D/H ratios in alkenones, *Paleoceanography*, *22*, PA4214, doi:10.1029/2007PA001468.

Peña, L., I. Cacho, P. Ferretti, and M. A. Hall (2008), El Niño–Southern Oscillation–like variability during glacial terminations and interlatitudinal teleconnections, *Paleoceanography*, *23*, PA3101, doi:10.1029/2008PA001620.

Rohling, E. J. (2007), Progress in paleosalinity: Overview and presentation of a new approach, *Paleoceanography*, *22*, PA3215, doi:10.1029/2007PA001437.

Rohling, E. J., and G. R. Bigg (1998), Paleosalinity and $\delta^{18}O$: A critical assessment, *J. Geophys. Res.*, *103*(C1), 1307–1318, doi:10.1029/97JC01047.

Rostek, F., G. Ruhland, F. C. Bassinot, P. J. Muller, L. D. Labeyrie, Y. Lancelot, and E. Bard (1993), Reconstructing sea-surface temperature and salinity using $\delta^{18}O$ and alkenone records, *Nature*, *364*(6435), 319–321, doi:10.1038/364319a0.

Rozanski, K., L. Araguas-Araguas, and R. Gonfiantini (1993), Isotopic patterns in modern global precipitation, in *Climate Change in Continental Isotopic Records*, *Geophys. Monogr. Ser.*, vol. 78, edited by P. K. Swart et al., pp. 1–36, AGU, Washington, D. C.

Schmidt, G. A. (1999), Error analysis of paleosalinity calculations, *Paleoceanography*, *14*(3), 422–429, doi:10.1029/1999PA900008.

Schmidt, G. A., A. N. LeGrande, and G. Hoffmann (2007), Water isotope expressions of intrinsic and forced variability in a coupled ocean-atmosphere model, *J. Geophys. Res.*, *112*, D10103, doi:10.1029/2006JD007781.

Schmidt, M. W., H. J. Spero, and D. W. Lea (2004), Links between salinity variation in the Caribbean and North Atlantic thermohaline circulation, *Nature*, *428*(6979), 160–163, doi:10.1038/nature02346.

Skinner, L. C., N. J. Shackleton, and H. Elderfield (2003), Millennial-scale variability of deep-water temperature and delta $\delta^{18}O_{dw}$ indicating deep-water source variations in the Northeast Atlantic, 0–34 cal. ka BP, *Geochem. Geophys. Geosyst.*, *4*(12), 1098, doi:10.1029/2003GC000585.

Stott, L., K. Cannariato, R. Thunell, G. H. Haug, A. Koutavas, and S. Lund (2004), Decline of surface temperature and salinity in the western tropical Pacific Ocean in the Holocene epoch, *Nature*, *431*(7004), 56–59, doi:10.1038/nature02903.

Strain, P. M., and F. C. Tan (1993), Seasonal evolution of oxygen isotope-salinity relationships in high-latitude surface waters, *J. Geophys. Res.*, *98*(C8), 14,589–14,598, doi:10.1029/93JC01182.

Werner, M., U. Mikolajewicz, M. Heimann, and G. Hoffmann (2000), Borehole versus isotope temperatures on Greenland: Seasonality does matter, *Geophys. Res. Lett.*, *27*(5), 723–726, doi:10.1029/1999GL006075.

A. N. LeGrande and G. A. Schmidt, NASA Goddard Institute for Space Studies, Columbia University, 2880 Broadway, New York, NY 10025, USA. (legrande@giss.nasa.gov)